Jpn. J. Appl. Phys. Vol. 35 (1996) pp. 3163–3166
Part 1, No. 5B, May 1996

Measurement and Analysis of Vibrations on Surface of Phantom Induced by Piezoelectric Extracorporeal Shock Wave Lithotripter

Yun-Seok JANG, Tetsuya AKASAKA[1], Michie SATO[1], Hiroshi KANAI[1] and Noriyoshi CHUBACHI[1]

Department of Electrical Engineering, National Fisheries University of Pusan, Korea
[1]*Department of Electrical Engineering,Faculty of Engineering, Tohoku University, Aramaki-aza-Aoba, Sendai 980, Japan*

(Received November 29, 1995; accepted for publication January 29, 1996)

We investigated the sound radiated from an object, induced by a piezoelectric extracorporeal shock wave lithotripter (ESWL). However, it was found that more direct measurement is necessary to analyze the sounds in piezoelectric ESWL. Therefore, we investigate the vibrations of a phantom, which are directly measured using laser Doppler velocimetry. The results show that the peak frequency in the power spectrum shifts as the number of shots increases from high frequency to low frequency. The previous results are confirmed by detecting the characteristic peaks obtained from the vibrations of bronze models. The bronze models are used to simulate the phantom during the breaking process. It is found that it is more difficult to make the models vibrate exactly at the focal point than above or below the focal region. These results will be applied to the monitoring of the breaking process and the choice of the optimum focal point on the calculus.

KEYWORDS: piezoelectric ESWL, breaking process, focal point, calculus, bending vibration

1. Introduction

We have already investigated the sound radiated from objects due to piezoelectric extracorporeal shock wave lithotripter (ESWL) in air in order to determine the phantom for a calculus at the focal point of piezoelectric ESWL. From those results, it was found that the phantom characteristics appear at the peak frequency of bending vibration in the power spectrum and there is a power change during the breaking process of the phantom.[1)] However, the characteristic peak cannot be detected during the breaking process. This indicates the measurement limit of sound radiated from underwater objects to the air induced by shock waves from piezoelectric ESWL.

Accordingly, we conclude that direct measurement[2,3)] is necessary to determine the exact generation mechanisms of the sound radiated from objects and vibrations of the objects due to shock waves from piezoelectric ESWL.

In this paper, we measure the vibrations of phantoms during the breaking process using laser Doppler velocimetry and analyze the characteristic variation of the peak frequency in the power spectrum. Next, we define a parameter to describe the relative position of the object with respect to the focal point of the ESWL and investigate the relationship between the power at the characteristic peak and the focal point on the object. Then, we describe the results of this investigation.

2. Vibration Measurements of Phantom during Breaking Process

First, we observe the phenomena associated with the fragmentation of the phantom due to piezoelectric ESWL and investigate why the radiated sound changes during the breaking process. In this experiment, a piece of chalk is employed as the phantom instead of the calculus itself because the acoustic impedance of chalk is almost equal to that of a urethral calculus. The acoustic impedance Z_{ca} of a urethral calculus is 6.25×10^5 kg/m^{2}s and that of the chalk employed in this experiment, Z_{ch}, is 6.13×10^5 kg/m^{2}s.[4)] The length and radius of cross section of the chalk are 6.2 cm and 0.5 cm, respectively. Figure 1 shows the configuration of the equipment and the phantom employed in the experiment. The phantom is laid on two rubber plates, 1 cm wide, separated from each other by a fixing tool. The shock waves are applied to the phantom at the focal point of the piezoelectric ESWL. Tape which reflects the laser beam is attached to the edge of the chalk away from the focal region as shown inside the circle in Fig. 1, because it is damaged or removed by the ESWL shock wave if it is attached at the focal point. The vibrations on the surface of the phantom are measured by laser Doppler velocimetry, the results of which are analyzed by a fast Fourier transform (FFT) analyzer.

The vibrations are measured from the first to the 1500th shock wave at intervals of 100 shots. The interval between the shock wave shots is 2 s. This interval is determined by the fact that cavitation bubbles[5–9)] induced by the shock waves remain near the focal point for about half a second. Figure 2 shows the waveforms and

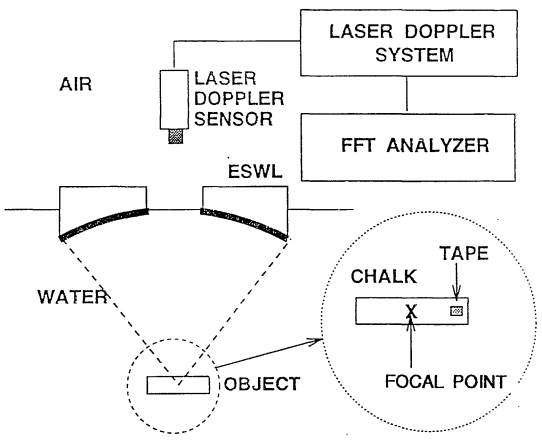

Fig. 1. The configuration of the laser Doppler velocimeter used to measure the vibration of phantoms induced by piezoelectric ESWL.

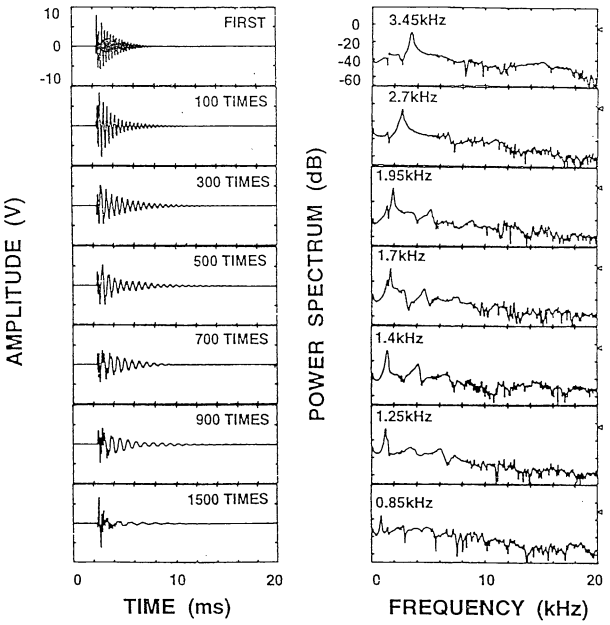

Fig. 2. The waveforms and power spectra of the vibrations detected when a shock wave is applied to a phantom by a piezoelectric ESWL during the breaking process.

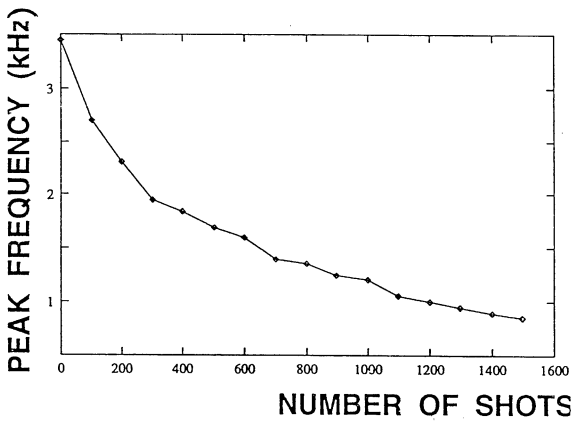

Fig. 3. Variation in peak frequency with number of shots during the breaking process.

spectra for the phantom vibrations measured by laser Doppler velocimetry. The results in Fig. 2 are taken at the first, 100th, 300th, 500th, 700th, 900th and 1,500th shock wave shot. We observe that the peak frequencies in the spectra vary with the number of shock wave shots, or the degree of fragmentation of the phantom. Figure 3 shows that the peak frequency varies as the number of shots increases from 3.45 kHz to 0.85 kHz. Therefore, it is possible that a sound of lower frequency than before is heard as the focal point of the phantom is gradually broken due to the increased number of shots.

3. Experiments with Model Phantoms during the Breaking Process

Next, the variation of the peak frequency during the breaking process is analyzed in detail. Bronze bars are used as the object to be shocked by piezoelectric ESWL. In the case of the chalk, we observed that the focal points

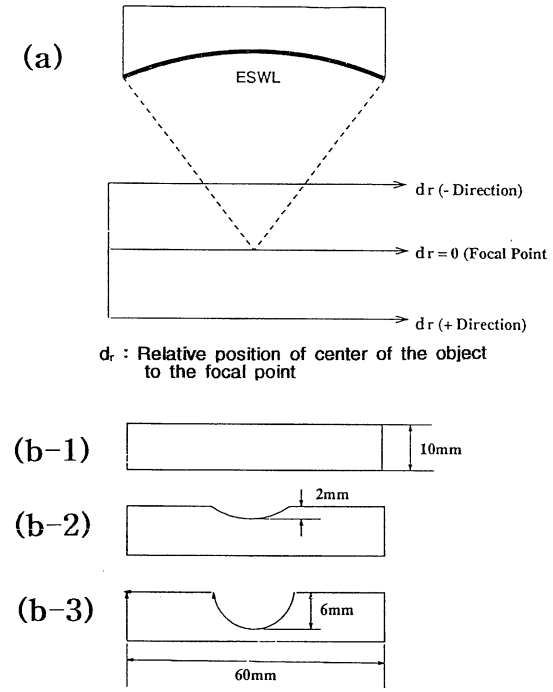

Fig. 4. (a) The relative positions of the model and the focal point of piezoelectric ESWL. The models used in our experiments simulated (b-1) the original shape, (b-2) the shape after about 200 shots and (b-3) the shape after about 600 shots.

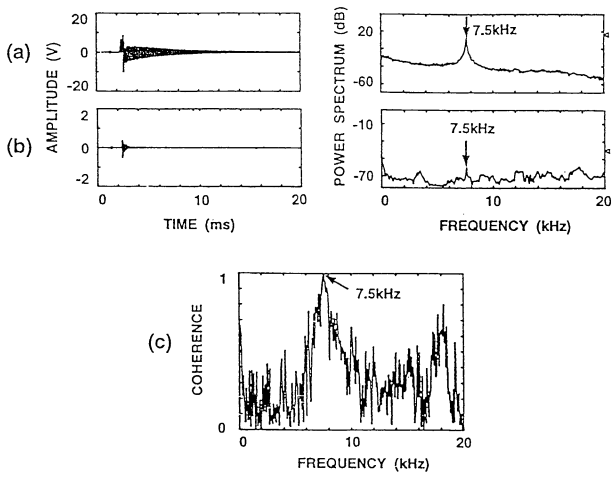

Fig. 5. The experimental results for the model in Fig. 4(b-1). (a) The waveform and the power spectrum of the vibration measured by laser Doppler velocimetry, (b) the waveform and power spectrum for the sound detected using the hydrophone and (c) the coherence between the spectra averaged 16 times.

of the phantom were removed as it was fragmented. Therefore, we assume three phantom shapes during the breaking process and model these phantom shapes by bronze bars as shown in Figs. 4(b-1)–4(b-3). The bronze model of the original shape in Fig. 4(b-1) is the same size as the chalk employed above. The length is 6.2 cm and the radius of cross section is 0.5 cm. The shapes after about 200 shots and 600 shots or more are assumed to be those as shown in Figs. 4(b-2) and 4(b-3). Figure 4(a) shows the relative positions of the model and the focal point of the ESWL. The parameter d_r is defined as

the relative position. $d_r = 0$ indicates that the center of the model exactly coincides with the focal point of the ESWL. When the center of the model lies in the direction of the ESWL from the focal point, d_r is negative. If it lies in the opposite direction, d_r is positive.

First, the vibrations of the models are measured at $d_r = 0$ by laser Doppler velocimetry and the sound radiated from the models is measured simultaneously using a hydrophone in the water. Figure 5 shows the experimental results for the model in Fig. 4(b-1). Figures 5(a) and 5(b) show the waveforms and spectra of the Doppler velocimetry and hydrophone signals, respectively. The coherence between the spectrum averaged 16 times of (a) and (b) is shown in Fig. 5(c). Clear peaks are observed at 7.5 kHz in the power spectra. The coherence at the same frequency has a value close to 1. This peak frequency coincides with the resonance frequency of the bending vibration, 7.6 kHz, which is theoretically calculated by[10]

$$f_n = \frac{a\lambda_n^2}{4\pi l^2} v_l, \quad (n = 1, 2, \ldots) \tag{1}$$

where $\lambda_1 = 4.73$, $\lambda_2 = 7.85$, $\lambda_3 = 10.99, \ldots$. l is the length, a is the radius of cross section, and v_l is the velocity of the longitudinal wave in the object. The velocity of longitudinal waves in bronze is 3,300 m/s when it is calculated theoretically. Figures 6 and 7 show the experimental results for the models in Figs. 4(b-2) and 4(b-3), respectively. Clear peaks in the spectra are observed at 6.9 kHz and 3.5 kHz and the coherence values are close to 1. From these results, it is clear that the thinner the model at the focal point the lower the peak frequency in the spectrum becomes. Figure 8 shows the variation in the peak frequency with the variation in thickness at the focal point. We conclude that the variation in the peak frequency in the experiment in §2 corresponds to the results of the experiment with bronze models in this section. Finally, we examine the variation in the power at the peak frequency by changing the value of d_r from -10 mm to $+10$ mm. The results are shown in Fig. 9. In the case of the models shown in Figs. 4(b-1) and 4(b-2), the power at the peak frequency decreases near $d_r = 0$. The vibration mode of the bar is considered in order to analyze this phenomenon. When a bar is free to move at both ends, the center of the bar is a node of mode

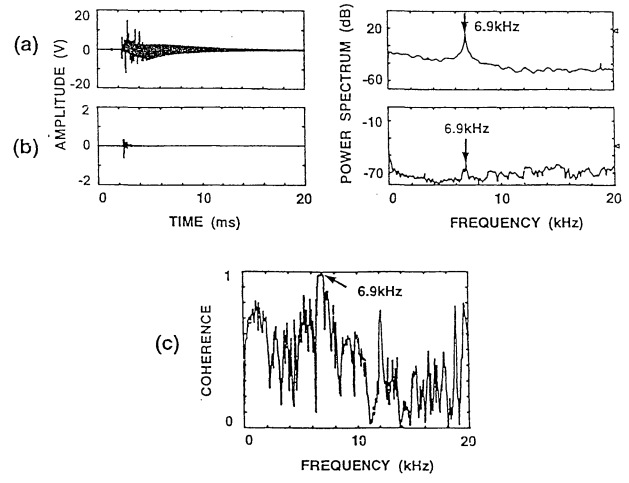

Fig. 6. The experimental results for the model in Fig. 4(b-2). (a) The waveform and the power spectrum of the vibration measured by laser Doppler velocimetry, (b) the waveform and the power spectrum for the sound detected using the hydrophone and (c) the coherence between the spectra averaged 16 times.

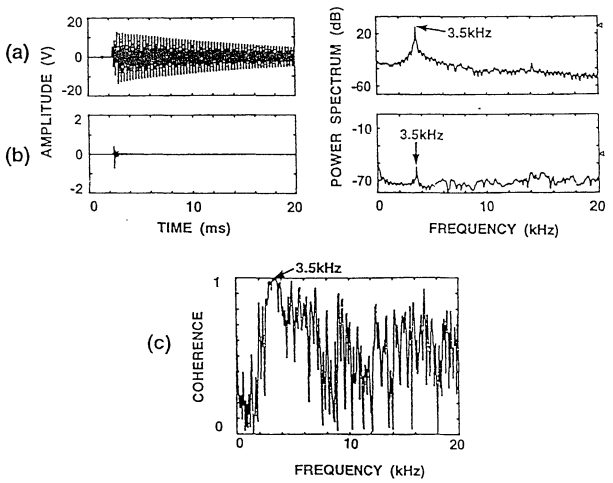

Fig. 7. The experimental results for the model in Fig. 4(b-3). (a) The waveform and the power spectrum of the vibration measured by laser Doppler velocimetry, (b) the waveform and the power spectrum for the sound detected using the hydrophone and (c) the coherence between the spectra averaged 16 times.

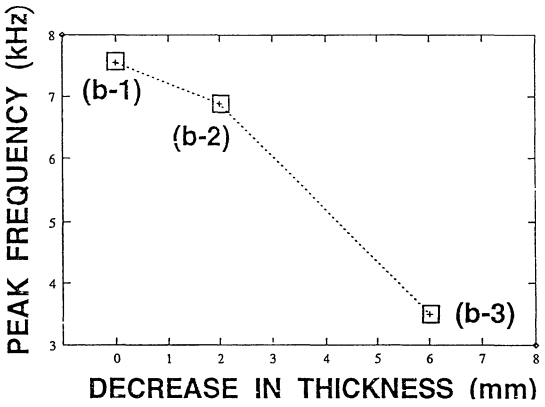

Fig. 8. The variation in the peak frequency due to the decrease in thickness at the focal point.

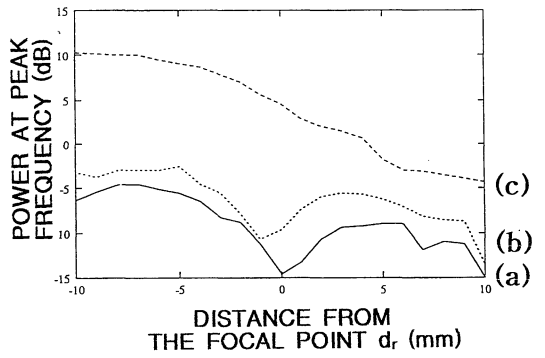

Fig. 9. The power at the peak frequency when the value of d_r is changed from -10 mm to $+10$ mm. (a) The results for the model in Fig. 4(b-1), (b) the results for the model in Fig. 4(b-2) and (c) the results for the model in Fig. 4(b-3).

2 bending vibration.[11] For this reason, it is difficult to make the center of the bar vibrate. From the experimental results, the power at the peak frequency at $d_r = 0$ is smaller than that at $d_r > 0$ or $d_r < 0$ in the focal region. This result indicates that it is more difficult to vibrate a bar-shaped object exactly at the focal point than above or below the focal point.

4. Conclusions

We report experimental results obtained by measuring the vibration on the surface of a phantom induced by piezoelectric ESWL and analyze these results by simulating the phantom using bronze models. From the results obtained in §2, the peak frequency in the power spectrum varies with the number of shock wave shots, that is, the degree of fragmentation of the phantom. It is found that the greater the number of shots, the lower the peak frequency in the power spectrum. Therefore, it is possible to hear sounds of lower frequency as the model is gradually broken due to the increased number of shots. The results of the experiments in §3 confirm those obtained in §2 using bronze models in order to determine the characteristics of each shape. Finally, we investigate the relationship between the power at the peak frequency and the position of the focal point. In order to define the relative positions of the models and the focal point, the parameter d_r is introduced. According to the results, the power at $d_r = 0$ is smaller than that at $d_r > 0$ or $d_r < 0$ in the focal region. It can be shown that it is more difficult to make the model vibrate exactly at the focal point than above and below the focal region. The results obtained in this paper will be applied to monitoring the breaking of calculi and the choice of the optimum focal point on the calculus.

1) H. Kanai, Y. S. Jang, N. Chubachi and Y. Tanahashi: Jpn. J. Appl. Phys. **33** (1994) 3159.
2) P. T. Hunter, B. Finlayson, R. J. Hirko, W. C. Voreck, R. Walker, S. Walck and M. Nasr: J. Urology **136** (1986) 733.
3) L. Olsson, L. O. Almquist, A. Grennberg and N. G. Holmer: Ultrasound Med. & Biol. **17** (1991) 491.
4) H. Asakage, Y. Aso, M. Tazaki, Y. Tanahashi, E. Higashihara and M. Yokoyama: *Shogekiha Kesseki Hasai no Subete* (All about Shock Wave Lithotripsy) (Toyo, Tokyo, 1991) p. 42 [in Japanese].
5) A. J. Coleman, J. E. Saunders, L.A. Crumand and M. Dyson: Ultrasound Med. & Biol. **13** (1978) 69.
6) C. C. Church: J. Acoust. Soc. Am. **86** (1989) 219.
7) N. Sanada, J. Ikeuchi, K. Takayama and O. Onodera: Proc. Int. Symp. Cavitation (1986) p. 67.
8) N. Ioritani, M. Kuwahara, K. Kambe, K. Taguchi, T. Saito, S. Shirai, S. Orikasa , T. Takayama and P. A. Lush: 17th Int. Symp. Shock Waves and Shock Tubes (1989) pp. 185–190.
9) A. R. Williams, M. Delius, D. L. Miller and W. Schwarze: Ultrasound Med. & Biol. **15** (1989).
10) T. Hayasaka and S. Yoshikawa: *Onkyo Sindoron* (Acoustic Vibration Theory) (Maruzen, Tokyo, 1974) p. 422 [in Japanese].
11) L. Kinsler, A. R. Frey, A. B. Coppens and J. V. Sanders: *Fundamentals of Acoustics* (John Wiley & Sons, New York, 1982) p. 75.